



Hollow wire corrosion of stainless steel ropes in a marine mooring system and its relation to microstructure

Paul Linhardt¹  | Maria V. Biezma²  | Roland Haubner¹  |
Roman Schuster³  | Tomasz Wojcik⁴ 

¹Institute of Chemical Technologies and Analytics, Technische Universität Wien, Vienna, Austria

²Departamento de Ciencia e Ingeniería del Terreno y de los Materiales, E.T.S.Náutica, Universidad de Cantabria, Santander, Spain

³Christian Doppler Laboratory for Interfaces and Precipitation Engineering CDL-IPE, Institute of Materials Science and Technology, Technische Universität Wien, Vienna, Austria

⁴Institute of Materials Science and Technology, Technische Universität Wien, Vienna, Austria

Correspondence

Paul Linhardt, Institute of Chemical Technologies and Analytics, Technische Universität Wien, Getreidemarkt 9/164, 1060 Vienna, Austria.
Email: Paul.Linhardt@tuwien.ac.at

Funding information

None

Abstract

Indications of corrosion were observed on ropes made of stainless steel type 316 in mooring systems of floating platforms in shallow tropical ocean water and doubts about the material quality came up. Routine investigations could confirm the type of alloy and the absence of sensitization, but the corrosion pattern was found unusual: individual wires of the ropes were found as hollow tubes many centimeters in length, which we refer to as hollow wire corrosion (HWC). Comparative investigations with a rope of the same specification from an arbitrarily chosen alternative producer revealed very similar susceptibility to chloride-induced pitting but a significant difference in repassivation behavior of the two products. An electrochemical test was designed which could reproduce HWC under realistic conditions with one product while the other repassivated readily. By electron backscattered diffraction, the different susceptibility to HWC could be related to the very different textures of the wire materials of the two products, resulting from different manufacturing technologies.

KEYWORDS

hollow wire corrosion, ropes, seawater, stainless steels, tunneling corrosion

1 | INTRODUCTION

The term “tunneling” was coined by Lennox^[1] more than 50 years ago in the context of corrosion of 304-type stainless steel (SS) wire ropes when analyzing the performance of such a rope from a marine buoy's mooring system. For distinguishing from pitting and crevice corrosion, “tunneling” was used to denote preferential corrosion along a rope's wire axis over some length. This failure pattern was observed at cross sections through the rope at arbitrary positions, revealing

individual wires being hollow with just a thin intact outer wall, while the core material was obviously etched out. No further attention was paid to the “tunneling” effect in this report and seemingly this phenomenon did also not receive much attention in the literature at later times, as was noticed by the authors during the research presented here.

Recently, corrosion of SS ropes from the mooring system of a floating platform was discovered by divers during a routine inspection by rust streaks emerging from a rope (Figure 1a). Such platforms, arranged in

This is an open access article under the terms of the Creative Commons Attribution-NonCommercial-NoDerivs License, which permits use and distribution in any medium, provided the original work is properly cited, the use is non-commercial and no modifications or adaptations are made.

© 2023 The Authors. *Materials and Corrosion* published by Wiley-VCH GmbH.

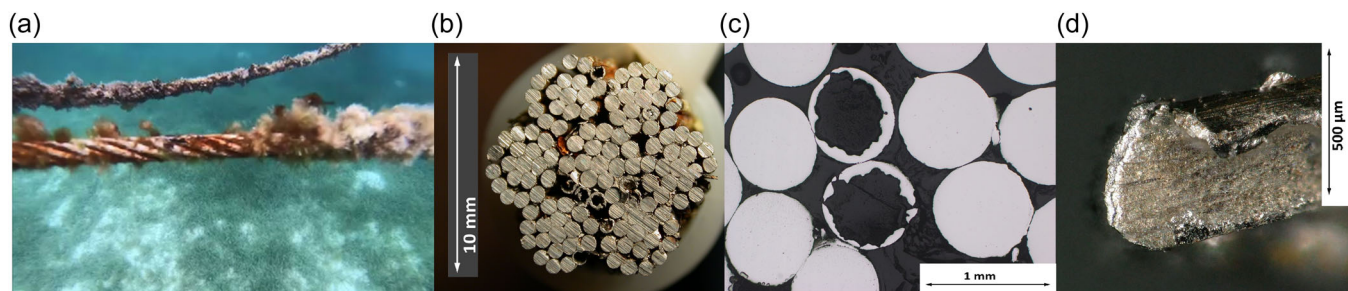


FIGURE 1 (a) Rusty stainless steel (SS) ropes with biofouling, as seen by a diver (created from a video). (b) View of a cross section through rope A1 with hollow wires, indicating tunneling corrosion. Rope configuration 7×19 : 7 strands with 19 wires each. (c) Close-up of hollow wires in the cross section. (d) Microscopic view of a single hollowly corroded wire from rope A1. [Color figure can be viewed at [wileyonlinelibrary.com](https://onlinelibrary.wiley.com/doi/10.1002/maco.202213699)]

arrays, are used in shallow tropical ocean waters and several such installations are in service independently in different locations. This finding of corrosion was unexpected since it was related to the platform in one location and had occurred after just a few months in service, while in two other, more than 100 km distant locations, no rust indications were noticed even after years of service.

Routine failure analysis confirmed that the ropes were indeed from the specified SS alloy (AISI 316) in all three locations, and local differences such as water pollution or platform construction could be ruled out to a high degree as reasons for the seemingly different behavior. In fact, it was found that the ropes from all three locations had suffered similarly from the tunneling corrosion introduced above (Figure 1b–d). There were just gradual differences in the length of the individual rope wires that were damaged throughout, making the difference in the visually detectable rust release observed by the divers. This problem of poor correlation between external visual appearance and degree of corrosion damage of SS ropes was already noted by Lennox.^[1]

Such poor experience in corrosion behavior inevitably leads to questions about the suitability of such material for the kind of application, or about the quality of the particular material. SS of alloy type 316, that is, the most commonly used molybdenum-bearing austenitic SS, is generally considered the lowest grade of seawater-resistant SS.^[2] In this sense, there is generally good experience with this alloy in many seawater applications, but a certain risk for corrosion failures under more critical conditions must be expected. Such critical conditions may be seen for ropes, where the densely packed wires not only create crevice conditions, but dynamic loading may also cause fretting between the wires. Consequently, corrosion processes may be expected to initiate easily by mechanical damage of the passive layer, and the ability of the material to re-passivate quickly despite the creviced configuration

appears decisive for long-term stability. According to Ref. ^[3] 316 type SS ropes may be considered for application in the sea atmosphere. Nevertheless, whether or not the risk for corrosion failure is finally acceptable in the complexity of a real application is today still a matter of practical experience in most cases and it was not the aim of this investigation to treat this question.

On the other hand, we found SS wires for ropes being standardized in their compositional, mechanical, and certain magnetic properties.^[3,4] Except with respect to sensitization,^[4] no requirements related to corrosion properties could be identified. Consequently, ropes of the same nominal specification may exhibit some variability in corrosion behavior from the compositional variations as permitted by standards, and from microstructural variations resulting from different production technologies. This research focused on the relationship between the microstructure of SS rope wires and their corrosion behavior, to understand the particular structural or environmental conditions under which tunneling corrosion may occur.

Since the term “tunneling corrosion” is nowadays frequently used in very different contexts, for the sake of clarity, we prefer the term “hollow wire corrosion” (HWC) in the following to denote the characteristic corrosion pattern as described above, that is, the selective corrosion of a wire’s core material, leaving behind a thin-walled, tube-like structure. We will support the justification for this specific term as this phenomenon turned out indeed being strongly related to the particular fabrication technology of wires.

2 | INVESTIGATIONS CARRIED OUT

The approach chosen in this work was on a comparative basis: three ropes from the field originating from one supplier (A), and one rope of the same nominal specification obtained from an arbitrarily chosen alternative source (C)

were subjected step by step to analytical, electrochemical, and microstructural investigations, as reported in the following. Finally, results will be compiled by correlating corrosion behavior and structural features.

2.1 | Material

All rope material used in this study was of 10 mm diameter in 7 × 19 configuration (Figure 1b) without retained lubricant, specified with a minimum breaking force of 52 or 57 kN depending on the supplier. They were nominally made from SS alloy AISI 316 (equivalent to mat. no. 1.4401 or X5CrNiMo17-12-2) that is, an alloy that is normally considered austenitic. The nominal diameter of the individual wires is 640 μm, and their minimum tensile grade should be 1625 MPa according to Ref.^[3] Such rather high tensile strength is obviously desired for a rope and considering typical data for fully austenitic, solution-annealed SS alloy 1.4401 (500–700 MPa^[2]), it points to the decisive role of the wire's microstructure for the mechanical properties of a SS rope. In fact, considering a drawing process as the base technology of wire fabrication, the formation of α'-martensite from austenite by cold working appears most plausible as a greatly strengthening component. However, since the production process of such wires may be a complex, multistage technology comprising of deformation and tempering steps, we may expect a wide variety of microstructures existing in rope products, all fulfilling the required macroscopic mechanical properties, finally.

Rope samples A1, A2, and A3 (between 20 and 100 cm long) were received from three mooring systems located at different islands in the Indian Ocean. They all suffered from HWC, with A1 being the most damaged one (Figure 1b–d) after only a few months in service, while the lesser damaged A2 and A3 had been in service for several years. These ropes were originally purchased independently for these applications, at different times, but from the same rope producer (which is not necessarily the producer of the wires). A1 was disassembled systematically over a length of ca. 40 cm and the damaged wires did not correlate with specific strands. Continuous HWC up to ca. 20 cm was observed which left a fragile, hollow, tube-like structure embedded in the rope body. Only a few wires were not affected at all. As to be expected from a dynamically loaded rope in a mooring system, fretting had occurred between the wires and Figure 2 presents such a location, which may be considered predestined for the initiation of pitting or crevice corrosion.

For comparison, rope sample C (20 cm long) from another producer also drawing the wires was used in the as-produced state.



FIGURE 2 Mark of fretting observed at a wire from rope sample A1. [Color figure can be viewed at [wileyonlinelibrary.com](https://onlinelibrary.wiley.com/doi/10.1002/maco.202213699)]

2.2 | Analysis of alloy composition

Noncorroded sections of the rope samples were analyzed by X-ray fluorescence (XRF) in vacuum using a wavelength dispersive spectrometer (Axios Advanced, Panalytical) operated at 50 kV. Results are presented in Table 1. No correction was made for the carbon content (nominally 0.07 wt.-%^[2]), which is not assessed by this analytical method. The alloy compositions of the samples appear very similar and there are no deviations from the requirements for alloy 1.4401 check analyses.^[2,3]

2.3 | Microstructural investigation by light optical microscopy

Short sections of rope samples A1, A2, A3, and C were embedded in phenolic resin, and cross sections were prepared by stepwise grinding and polishing finally by 0.3 μm alumina paste. Lichtenecker-Bloech etchant,^[5] applied for 3 min, was found to provide the most useful information in light optical microscopy; see Figure 3. The wires of C appear homogenous across the diameter with just some small, feathered structures close to the center. By contrast, the wires of A1, and gradually lesser those of A2 and A3, exhibit a nonevenly distributed microstructure with a wide, diffuse and dark zone of mostly rhombic shape in the center. The selected etchant reveals austenite bright, while martensite and/or ferrite appear dark. Consequently, these results indicate strong gradients in the distribution of presumable martensite for A-wires, while the small inhomogeneity in the center of C material remains unidentified. It was not possible to achieve clearly defined microstructural resolution by light microscopy, indicating a high degree of deformation.

TABLE 1 Results of X-ray fluorescence analysis of rope samples A1, A2, A3, and C, in wt.-%.

Sample	Fe	Cr	Ni	Mo	Mn	S	P	Si	Cu	Ti	Nb	V	Co	Total
A1	67.96	16.87	10.97	2.15	1.08	n.d.	0.04	0.41	0.27	0.01	n.d.	0.06	0.19	100
A2	67.95	16.73	11.07	2.28	0.93	n.d.	0.04	0.39	0.42	n.d.	0.01	0.05	0.14	100
A3	68.34	16.51	11.00	2.27	0.87	n.d.	0.04	0.39	0.4	n.d.	n.d.	0.06	0.12	100
C	67.66	16.90	11.14	2.34	0.98	n.d.	0.04	0.48	0.32	n.d.	n.d.	n.d.	0.12	100

Note: Carbon content not analyzed. (n.d. = not detected).

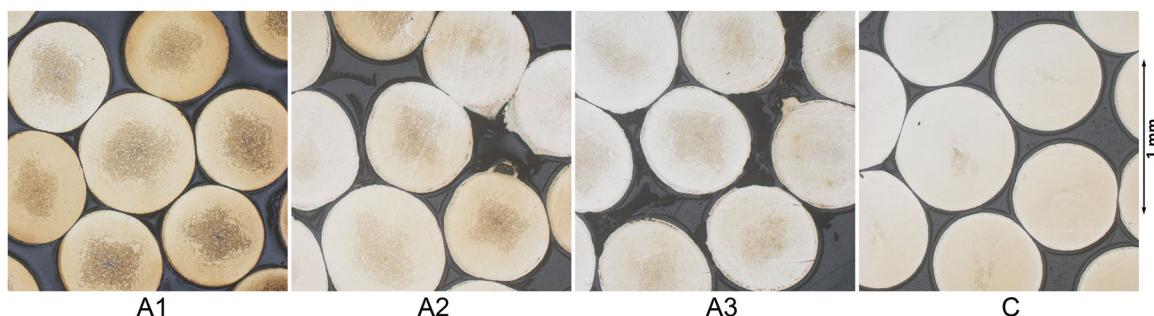


FIGURE 3 Metallographically prepared cross sections of ropes A1, A2, A3, and C in the light optical microscope. Etchant: Lichtenecker-Bloech. [Color figure can be viewed at [wileyonlinelibrary.com](https://onlinelibrary.wiley.com/doi/10.1002/maco.202213699)]

TABLE 2 Magnetizability of the wires from rope samples A1, A2, A3, and C, in wt.-% referring to iron.

sample	A1	A2	A3	C
Sample weight (g)	1.1793	1.2289	1.2529	1.0933
Magnetizability (wt.-%)	4.193 ± 0.042	3.633 ± 0.006	2.821 ± 0.008	9.470 ± 0.045

2.4 | Determination of magnetizability

Noncorroded wires were randomly selected from each rope sample and cut into 10–30 mm long pieces, summing up to roughly 1 g. These pieces were bundled and measured in a FOERSTER Koerzimat CS 1.096. Six repetitive measurements per sample were done and Table 2 provides the results given in wt.-% of magnetizable material, referring to pure iron as 100%. As is indicated by the data and as expected, a significant amount of nonaustenitic, magnetically susceptible component is present in the wires, particularly in rope C.

It may be noted that an additional 0.79 g wires of C were solution annealed in nitrogen atmosphere at 1050°C for 1 h, water quenched, and also subjected to such a measurement. The signal was below the sensitivity of the instrument, that is, <0.1 wt.-%, indicating the expected full conversion of this alloy to austenite by such thermal treatment.

2.5 | X-ray diffraction (XRD)

Wires from rope sample A1 were subjected to XRD analysis. In a first attempt, a Bruker D2-Phaser and a Bruker D8-Advance were adapted for the measurement of a straight steel wire and a planary-coiled wire, respectively, in reflection configuration (Bragg-Brentano geometry). Cu K_{β} radiation was used in the range 20–120° (2 θ) and the evaluation of diffractograms involved Rietveld refinement. While with the straight wire pure austenite phase was detected, the more sensitive coiled wire configuration indicated a certain additional amount of martensite/ferrite (not distinguishable by XRD).

These results indicate austenite being located preferentially at the wire's surface, while martensite (ferrite) is rather accumulated in the core of the wire. Consequently, a further XRD analysis focusing on the center of a cross-sectioned wire was carried out, employing Empyrean equipment from Panalytical. At the primary

side, a parallel beam mirror, $\frac{1}{2}^\circ$ divergence slit, 0.04 rad Soller slit, and a $300\ \mu\text{m}$ micro-focus adapter were applied, targeting the center of the ca. $640\ \mu\text{m}$ wide polished face of a wire. At the secondary side, a Gallipics detector was used and $\text{Cu K}_{\alpha(1,2)}$ radiation was detected between 41.5° and 84° (2θ) at step size 0.0143° . Data evaluation involving Rietveld refinement yielded a 75.4% austenite to 24.6% martensite (ferrite) ratio and the observed peak broadening points to significantly distorted crystal structure. No indications for any further phase were detected.

2.6 | Energy dispersive X-ray analysis (EDX)

For assessing the distribution of chromium across the diameter of A1 wires, polished cross sections of 2 different noncorroded wires were analyzed by EDX (EDAX-Sapphire) in the scanning electron microscope (Philips XL-30, operated at 20 kV). Analyses across spots of $60 \times 80\ \mu\text{m}$ from the center and from near the rim yielded for this method practically identical chromium concentrations (raw data for rim/center in at.-%: 18.0/17.9 and 18.3/18.4). Consequently, significant chromium depletion at a large scale could be ruled out as the cause of preferential axial corrosion.

2.7 | Testing for sensitization

To assess possible chromium depletion at the microstructural scale, noncorroded wire sections from all rope samples were subjected to the electrochemical potentiokinetic reactivation test (EPR-, Cihal-Test, based on^[6]). Each wire was embedded in epoxy resin and the cross-section area ($0.32\ \text{mm}^2$) was ground to grit #320. These specimens were used as working electrodes, together with a counter electrode (platinum wire), and a mercury-mercury sulfate (MMS, in sat. potassium sulfate) reference electrode, for recording potentiodynamic scans in 75 ml sulfuric acid (0.5 M) with potassium thiocyanate (0.01 M) as the activator.^[7] A computer-controlled Bank POS-1 (Germany) potentiostat was used to scan at $1.67\ \text{mV/s}$ from the open circuit potential (close to $-750\ \text{mV}_{\text{MMS}}$, established after 15 min) in anodic direction well into the passive range ($-50\ \text{mV}_{\text{MMS}}$) and then back to $-750\ \text{mV}_{\text{MMS}}$.

The results are presented in Figure 4 and the absence of any anodic current peak during the reverse scan indicates that none of the wire materials suffers from local chromium depletion, that is, some kind of sensitization may be excluded as the cause for the preferential corrosion along the wire core.

2.8 | Testing for pitting corrosion

The susceptibility to pitting corrosion of all rope samples was tested with noncorroded wires, which were cleaned and degreased (but not abraded) at the outer surface and the face at one end was ground wet by hand stepwise to grit #1000. The specimen was immersed vertically with the ground face down ca. 15 mm deep into artificial seawater (75 ml, prepared according to Ref. ^[8]), acting as the working electrode. A platinum wire was used as the counter electrode, and a silver-silver chloride electrode (SSE, in sat. potassium chloride) acted as the reference electrode. Potentiodynamic scans were recorded by using a computer-controlled Bank POS-1 (Germany) potentiostat, starting at the open circuit potential which was allowed to equilibrate overnight. At a rate of $0.167\ \text{mV/s}$, the potential was scanned in the anodic direction and the scan was reversed when the current had reached $+1\ \text{mA}$. Scanning in the cathodic direction was continued until the current got cathodic. All tests were made at least in duplicate and yielded essentially very similar results. For the sake of clarity, only one result per sample type is presented in Figure 5a.

From the curves in Figure 5a, we see that the critical pitting potentials (E_{pit}) of all wires fall into a remarkably narrow potential window ($560\text{--}620\ \text{mV}_{\text{SSE}}$ at an arbitrarily chosen current of $10\ \mu\text{A}$), indicating that all specimens have very similar susceptibility to pitting. By visual examination after the test, the locations of the pits were found randomly distributed and preferential attack at the core material at the wire's face was not observed. It should be noted that also the 3-phase-boundary air/wire/

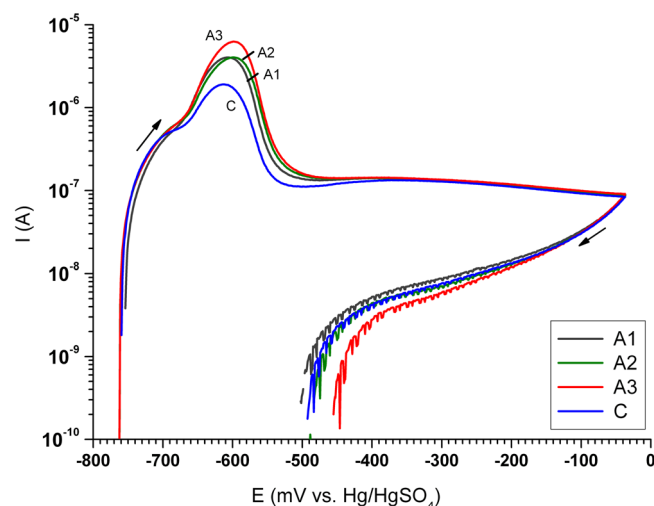


FIGURE 4 Electrochemical potentiokinetic reactivation test results gained at cross sections ($0.32\ \text{mm}^2$) of wires from samples A1, A2, A3, and C (only anodic currents are displayed). [Color figure can be viewed at wileyonlinelibrary.com]

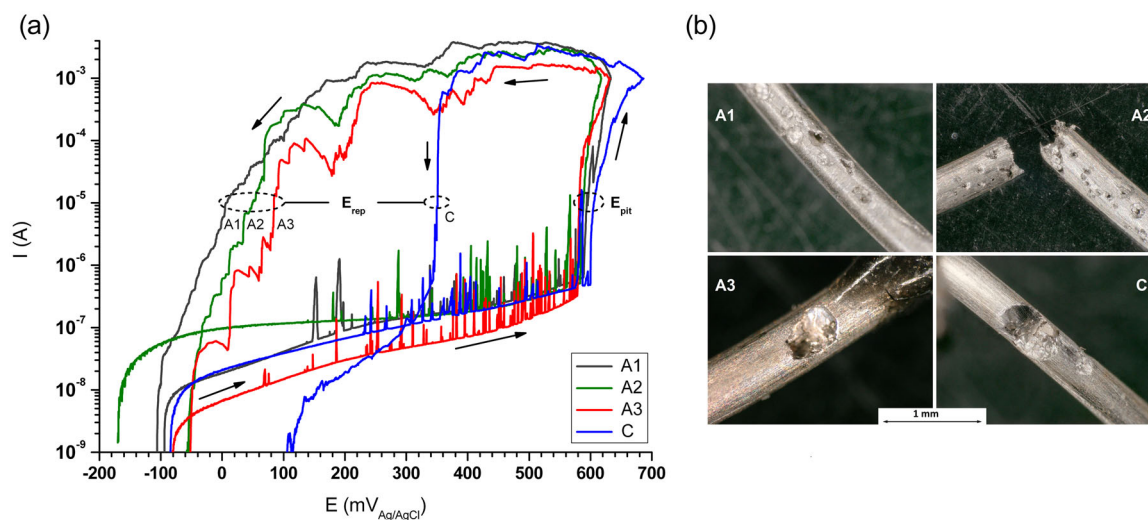


FIGURE 5 (a) Potentiodynamic scans of wires from samples A1, A2, A3, and C in artificial seawater, indicating E_{pit} and E_{rep} . (b) Pitting observed at the wires after the potentiodynamic test. [Color figure can be viewed at [wileyonlinelibrary.com](https://onlinelibrary.wiley.com/doi/10.1002/maco.202213699)]

electrolyte was not the preferential site of the attack in these tests. On the other hand, the ability to repassivate, that is, the repassivation potential E_{rep} , was found significantly different between A1, A2, A3, and C wires. Considering the current level of $10 \mu\text{A}$, all tested C wires dropped below this value during the cathodic scan at potentials more anodic than $+250 \text{ mV}_{\text{SSE}}$, while all A-type wires did not above $+110 \text{ mV}_{\text{SSE}}$, and specifically A1 not above $0 \text{ mV}_{\text{SSE}}$. This may be considered an indication of the ability to repassivate being a significant parameter for discriminating the corrosion properties of the SS rope wires.

Examination of the wires, particularly of A1, by digital microscopy (Keyence VHX-100), yielded no clear signs of HWC; see Figure 5b. The pits showed the usual undercutting, but the preferential growth in the axial direction could not be observed unambiguously. However, this may become plausible by taking into account the total amount of metal dissolved in such an experiment: For a simplified alloy composition (Fe with 18 wt.-% Cr and 10 wt.-% Ni), with the usual number of electrons consumed (Fe:2, Cr:3, Ni:2), considering an average density for stainless steel (7.9 g/cm^3), and by applying second Faraday's law, we may estimate that a charge of 30.2 As/mm^3 are required for dissolving the SS anodically. By integrating the current data of the potentiodynamic scan with wire A1 (Figure 5a), a total anodic charge of 7.28 As can be estimated, corresponding to 0.241 mm^3 . For the wire diameter of $640 \mu\text{m}$, this means that in total material corresponding to a wire length of $750 \mu\text{m}$ has got dissolved during the experiment, which is in the order of the diameter. Since the pit growth direction even in homogenous SS is

governed by complex processes, as was summarized and demonstrated recently,^[9] we may conclude that potentiodynamic experiments are not necessarily suitable for replicating HWC distinguishable from pitting since the amount of dissolved metal is insufficient.

2.9 | Testing for HWC

Based on the experiences from potentiodynamic experiments, a test was designed making use of the potential switching technique: In the first phase, pitting corrosion should be initiated and stabilized by polarizing sufficiently high above E_{pit} for some time. This phase was defined by 3 h at $E_{\text{pitinit}} = +750 \text{ mV}_{\text{SSE}}$. In the second phase, active corrosion may be maintained for some time at a less anodic potential E_{growth} , which should be above E_{rep} (the highest E_{rep} of $+320 \text{ mV}_{\text{SSE}}$ was observed for wire C, see Figure 5). On the other hand, E_{growth} should also be not too far from practically relevant potentials of SS in the marine environment, which are known to approach values up to $+350 \text{ mV}_{\text{SSE}}$ due to the microbial effect of “ennoblement.”^[10] Consequently, and to make the test slightly harsher, this phase was defined by $E_{\text{growth}} = +400 \text{ mV}_{\text{SSE}}$ and 24 h duration.

For this test, a multichannel potentiostat (Octopoti, home-made^[11]) was utilized, which offers the following beneficial features: (i) parallel testing of eight wires at the same potential in one shared electrolyte container, and (ii) current limitation for each channel by design, with a cutoff at $I_{\text{lim}} = 1.2 \text{ mA}$ in the instrument configuration applied here. Such a current limitation is considered realistic, since the limited kinetics of cathodic reactions and the electrolyte

resistance between local anodes and widely distributed cathode areas will limit the current, particularly in the crevice configuration in the inner part of a rope. Data acquisition was set to log every 5 min the desired potential (E_{set}), and for each of the eight specimens data on current (I) and the deviation of its potential from E_{set} value (dE). The value of dE is necessarily zero in the potentiostatic mode but provides the corresponding values when current limitation triggers and I_{lim} is maintained by adapting the specimen's potential.

Per test, eight noncorroded wires (ca. 35 mm) were retrieved as randomly as possible from a rope sample (A1, A2, A3, and C), cleaned, degreased, and clamped to a sample holder for contacting as working electrodes. The sample holder, arranged in a 2×4 array with 7.5 mm spacing, allows for immersing all wires vertically in the electrolyte. The electrolyte was 2 L of artificial seawater,^[8] kept in a cylindrical container (ca. 20 cm diameter), and a SS mesh adapted to the container wall served as the counter electrode. The working electrode array was positioned in the center of the container and the tip of the reference electrode (SSE) was placed aside.

Since the graphical compilation of all data appears not feasible, the typical result of a single wire of A1, qualitatively also representing A2 and A3, and the result of one wire representing all of C, are presented in Figure 6. They will be explained in the following while Table 3 presents the summary by some derived quantities.

As we see from Figure 6, the test starts with applying E_{pitinit} and active corrosion is initiated for all wires practically instantaneously. I_{lim} is maintained by the instrument by lowering the potential (dE) suitably. With time, dE shifts to more negative for both wire types, indicating increasing activation. However, during the end of this first phase, dE of A1 exhibits a smoother trend and tends to have more negative values compared to that of C. The final dE values of all wires at the end of this phase (i.e., after 3 h) were evaluated by extracting the most positive (max.), the most negative (min.), and estimating the average (avrg.); see Table 3. These data indicate A1 dissolving more easily (at lower anodic potential) and more steadily (smaller fluctuations in potential) compared to C, with A2 and A3 being similarly prone to corrosion as is A1. After this phase, all wires have experienced an equal predamage by an anodic charge of 12.96 As, equal to a metal loss of 0.43 mm^3 and accompanied by the corresponding electrolyte acidification inside the pits.

In the second phase of the test, polarization is lowered to E_{growth} and maintained for 24 h. As indicated in Figure 6, the wire of A1 maintains I_{lim} with dE around -200 mV for ca. 7 h before the current drops and fluctuates between $300 \mu\text{A}$ and 1 mA (with dE necessarily at zero) throughout the rest

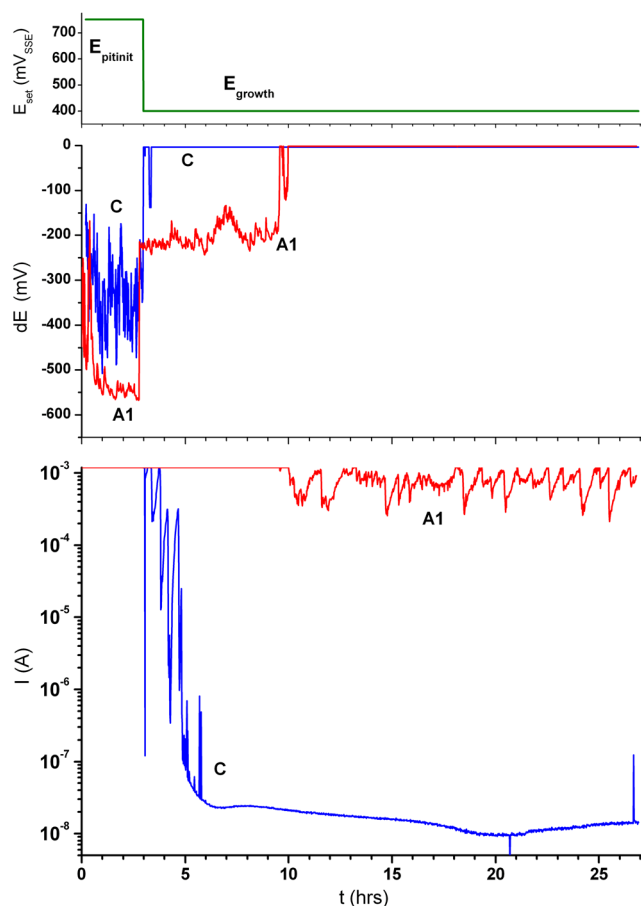


FIGURE 6 Switched potentiostatic hollow wire corrosion-test results for one wire of A1 and one wire of C, in artificial seawater. [Color figure can be viewed at wileyonlinelibrary.com]

TABLE 3 Characteristic data extracted from hollow wire corrosion-test results.

Sample	A1	A2	A3	C
Phase 1: $E_{\text{pitinit}} = +750 \text{ mV}_{\text{SSE}}$				
dE (mV)	Max. -566	-406	-554	-138
	Avrg. -602	-586	-593	-280
	Min. -629	-650	-624	-385
Phase 2: $E_{\text{growth}} = +400 \text{ mV}_{\text{SSE}}$				
dE (mV)	Avrg. -233	-169	-195	-2
Q_a (As)	Max. 103.8	103.8	103.7	9.64
	Avrg. 99.94	95.4	96.8	4.5
	Min. 78.2	76.4	87.8	0.03
Remarks	1 wire broken		3 wires broken	All wires passivated

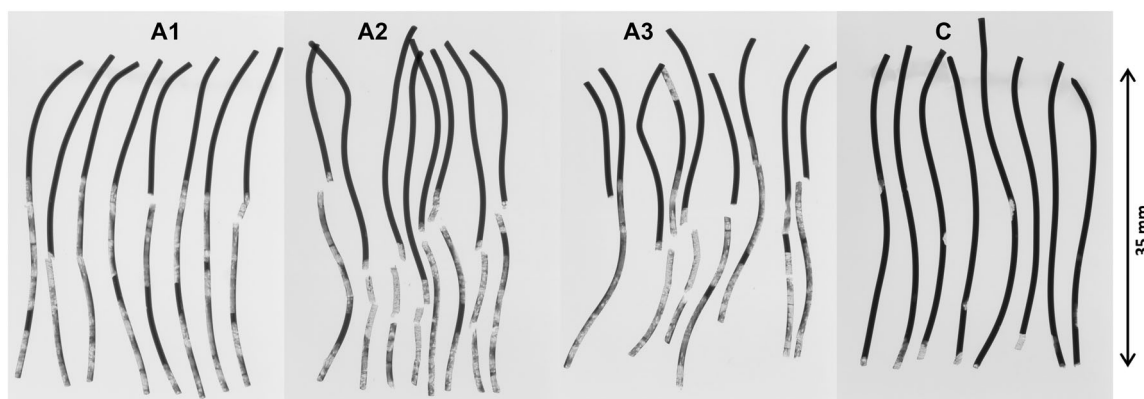


FIGURE 7 Radiographs of hollow wire corrosion-tested wire specimens.

of the experiment. By contrast, the current of C drops within 3 h by orders of magnitudes and maintains a level of a few 10 nA for the rest of the experiment. This indicates spontaneous passivation and stable passivity at the applied potential of +400 mV_{SSE} ($=E_{\text{growth}}$ with $dE = 0$). During this test phase, one wire of A1 and three wires of A3 broke off and their data were not considered for the following comparative evaluation: Table 3 presents the average dE values for all wire types, indicating that A1 wires were most easily dissolved anodically, followed by A3 and A2, while C wires did hardly deviate from E_{growth} due to their passive state during most of the time. This is also reflected in the anodic charge (Q_a) obtained by integrating the current from $t = 3$ to $t = 27$ h: While C wires consumed an average of just 4.5 As with 9.64 As for the most damaged specimen, even the most corrosion resistant specimen of A (A2) consumed 76.4 As. The ranking of A1 being the least resistant material, followed by A3 and A2 is again reflected in the average values for Q_a , which are close to the theoretical maximum (I_{lim} for 24 h = 103.7 As).

2.10 | Radiography of HWC-tested wires

All specimens from the potentiostatic switching test were subjected to radiography using a Viscom X8060 scanner with a Viscom XT9190-THP X-ray tube operated at 90 kV and 100 μ A. 14-bit intensity resolution is provided and 1400 ms exposure time was used.

Figure 7 presents the radiographs, which indicate clearly that HWC was reproduced for the wire types A1, A2, and A3. There is quantitative material loss over 20–30 mm in the inner of the wires, which appeared as highly fragile, thin-walled tubes with shiny outer surfaces after the test. By contrast, the specimens of C are damaged by pitting corrosion and max. 3 mm deep HWC emerges from the end face of the specimens. However, most of this damage of C must be related to the forced corrosion

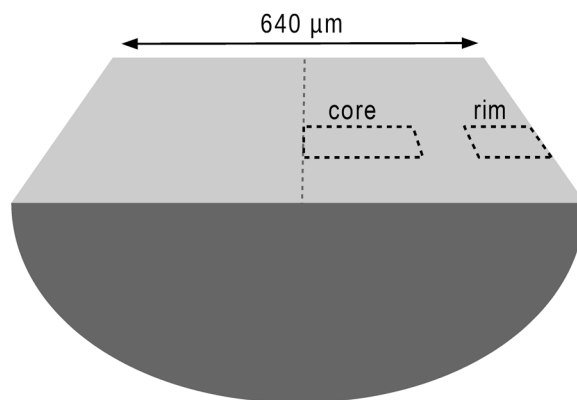


FIGURE 8 Schematic of the core and rim areas in a wire's longitudinal cross section addressed by electron backscattered diffraction scans (not to scale).

conditions in the first test phase at E_{pitinit} , since 0.43 mm^3 have been dissolved there, compared to $0.001\text{--}0.32 \text{ mm}^3$ at E_{growth} in the second phase, as may be estimated from Q_a min./max. data in Table 3.

2.11 | Structural analysis by electron backscatter diffraction (EBSD)

EBSD analysis of A1 and C wires was performed on a ZEISS Sigma 500 VP scanning electron microscope equipped with a field emission gun, operating at 15 kV acceleration voltage, and using an EDAX Velocity EBSD camera. As indicated in Figure 8, cross-sectional areas located parallel to the wire axis extending from the center and to the rim of the wire were chosen for the investigation. EBSD scans were obtained with step sizes of 0.1 and 0.08 μ m for the outer and inner regions of the wire, respectively. EBSD data clean-up was performed with the EDAX OIM Analysis 8.0 software. The Matlab Toolbox MTEX 5.8 was used for EBSD data analysis.

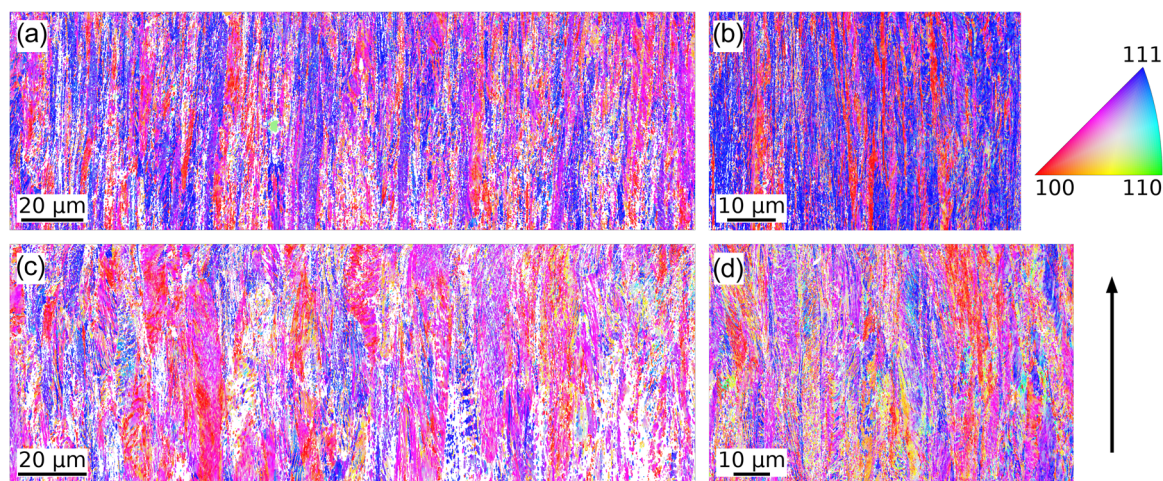


FIGURE 9 Electron backscattered diffraction inverse pole figure maps of austenite colored with respect to the wire drawing direction (indicated by the arrow) for the core (a) and rim (b) region of sample A1, and core (c) and rim (d) region of sample C, as indicated in Figure 8. The A1 sample shows a typical fcc wire drawing microstructure and texture with $\langle 111 \rangle$ (blue) and $\langle 100 \rangle$ (red) components. The C sample shows a twisted microstructure with a much weaker texture that significantly deviates from the texture in the A1 sample. [Color figure can be viewed at wileyonlinelibrary.com]

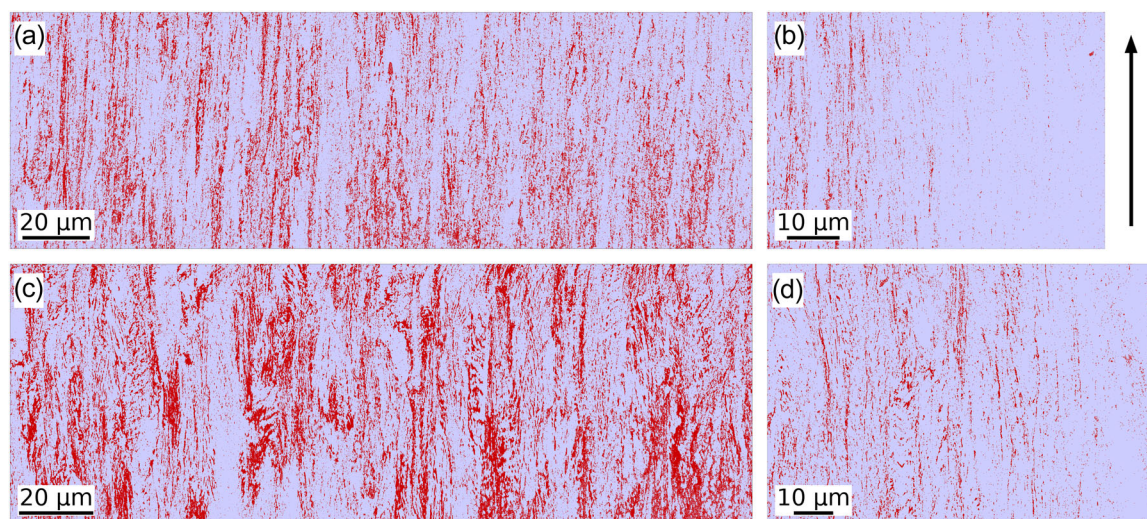


FIGURE 10 Electron backscattered diffraction phase maps presenting austenite in blue (bright) and martensite in red (dark), for core (a) and rim (b) region of sample A1, and core (c) and rim (d) region of sample C, as indicated in Figure 8. The arrow indicates the wire drawing direction. [Color figure can be viewed at wileyonlinelibrary.com]

The microstructure in the A1 specimen consists of a matrix of austenite grains elongated along the drawing direction (Figure 9a,b). The cross section of the austenite grains is about $1\text{--}3\ \mu\text{m}$ wide. Thin martensite strands extend between austenite grains, where the martensite phase fraction is about 15% in the wire core (Figure 10a,b). Toward the wire rim, the martensite density decreases and is close to zero in the outermost $50\ \mu\text{m}$. The austenite grains exhibit a pronounced texture with two dominant texture components typical for fcc materials processed by wire drawing.^[12,13] In the primary component one $\langle 111 \rangle$

direction is parallel to the drawing direction, while for the secondary component one $\langle 100 \rangle$ direction is parallel to the drawing direction (Figure 11a,b). By software-based comparison of the orientation of the martensite grains with the orientation of the neighboring austenite grains, it was found that they adhere to the common Kurdjumov–Sachs or Nishiyama–Wassermann orientation relationships^[14–16] and thus inherit a pronounced texture from the austenite matrix.

By contrast, the microstructure in the C specimen is notably distorted compared to the conventional wire

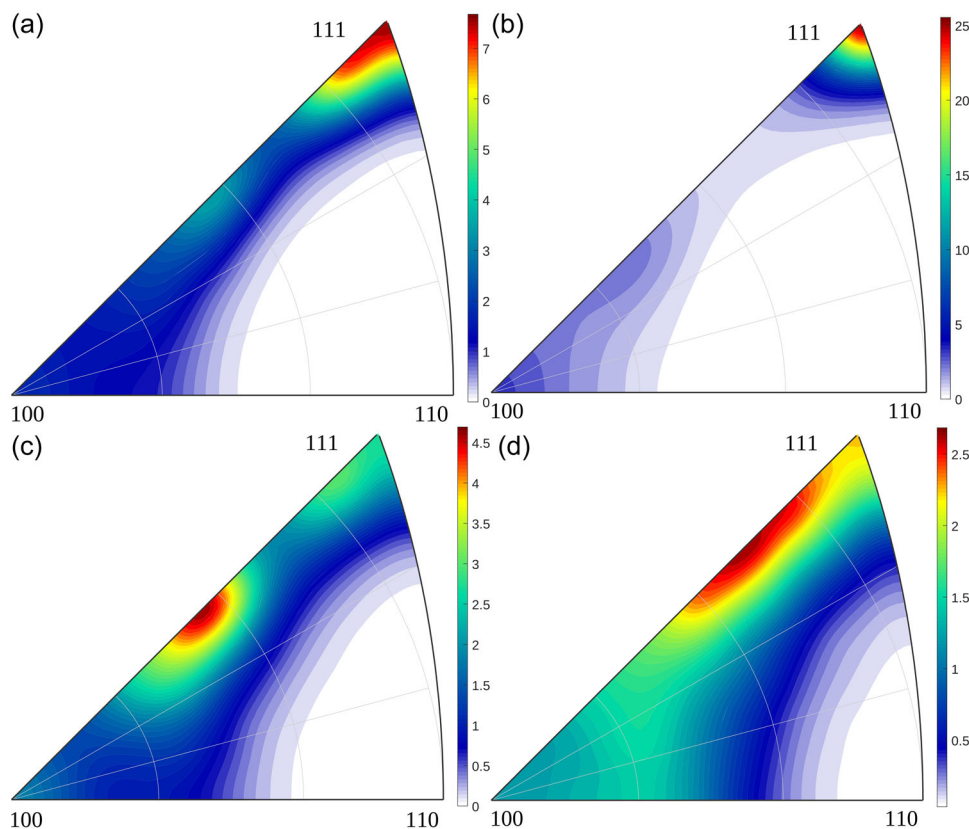


FIGURE 11 Inverse pole figures of austenite calculated from electron backscattered diffraction data from core (a) and rim (b) region of sample A1, and core (c) and rim (d) region of sample C, as indicated in Figure 8. The color code represents the respective densities of austenite crystallographic directions parallel to the wire drawing direction, where the numerical values indicate how frequent orientations occur compared to a randomly oriented sample. Sample A1 shows a strong preference for $\langle 111 \rangle$, which occurs over 7 and 25 times more often in the core and rim regions, respectively, than for a random orientation distribution. Sample C shows a much weaker preference for directions around $\langle 225 \rangle$ in the core and between $\langle 225 \rangle$ and $\langle 111 \rangle$ in the rim. [Color figure can be viewed at [wileyonlinelibrary.com](https://onlinelibrary.wiley.com)]

drawing microstructure seen in the A1 sample (Figure 9c,d). The austenite grains form about $10\ \mu\text{m}$ thick bands that are twisted around the drawing direction. The martensite domains, which make up about 24% of the area in the core, are thicker and patchier compared to the A1 sample (Figure 10c,d). In the outer region the martensite bands are thinner and less frequent, and in the outermost $30\ \mu\text{m}$ martensite is rare. The austenite texture significantly deviates from the texture observed in A1. In the core, the most frequent direction parallel to the drawing direction is $\langle 225 \rangle$ (Figure 11c,d). Toward the rim, the texture is significantly less pronounced and shows a distribution of preferred axes parallel to the drawing direction that ranges from $\langle 225 \rangle$ to $\langle 111 \rangle$. The martensite domains in the C sample were likewise found to exhibit a significant spread of orientations. Comparison of the martensite orientations with the orientations of neighboring austenite grains also indicated that their orientation relationships moderately deviate from the Kurdjumov–Sachs and Nishiyama–Wassermann relationships.

3 | DISCUSSION

The alloy compositions of the samples A1, A2, A3 from the one supplier, and C from the alternative one, as provided by XRF (Table 1), confirm their compliance with 1.4401/AISI 316 specification and the just small differences make them appear well suited for further comparative investigations. On the other hand, the metallographically prepared cross sections (Figure 3) indicate a significant difference between the A1, A2, A3, and C samples: While C appears rather homogenous, the A samples present in the center a diffuse, zone of rhombic shape. This pattern is most pronounced with A1 and EDX analysis confirmed that it is not related to an uneven distribution of chromium. As the etchant applied in metallography makes martensite appear dark in a bright austenite matrix, we may assume that this pattern reflects the distribution of martensite in the wire. Its rhombic distribution in all three A samples may be an indication of their origin from the same wire production technology, possibly even from the same producer.

The presence of the ferromagnetic martensite in the nonmagnetic austenite is quantitatively reflected in the magnetizability (Table 2). The ranking of these values by $A1 > A2 > A3$ seems to correspond with the visual impression from the etching pattern in Figure 3a–c, while C, yielding the highest magnetizability, appears surprisingly bright in Figure 3d. The results from the XRD investigation with A1 confirm a high fraction of martensite accumulated around the wire's axis, while the outer shell is predominantly austenitic. This finding of an austenitic shell coincides with the observation made with all wires in the metallographic investigation (Figure 3: the outer shell appears bright) and is consistent with the result from EBSD analysis for samples A1 and C (Figure 10).

Since the manufacturing technology of the rope wires is unknown to us, sensitization, that is, chromium depletion along grain boundaries due to annealing steps, could not be ruled out as a possible reason for HWC. However, the results of the EPR-test (Figure 4) demonstrate that none of the wire samples is in the sensitized state.

The susceptibility of the wires to chloride-induced pitting corrosion was assessed by potentiodynamic scans (Figure 5) and very similar values for E_{pit} were found. It may be surprising that the face of the wires, where the martensite gets in contact with the electrolyte, was not preferentially attacked and there is no correlation of E_{pit} with the amount of martensite present in the wires as derived from the magnetizability data in Table 2. However, this is in good agreement with the findings reported quite some time ago^[17] and stated again more recently^[18] for molybdenum-free austenitic SS of type 304/1.4301 (CrNi 18/9), where martensite from deformation was found not to increase the susceptibility to pitting corrosion. On the other hand, it was demonstrated by Keller et al.^[17] that the martensite gets dissolved preferentially under acidic conditions and particularly in the acidic pit electrolyte as is formed during active pitting corrosion.

Since the limited amount of metal dissolved during potentiodynamic tests does not allow for differentiating doubtlessly regular pitting from HWC, the potentiostatic HWC-test in artificial seawater was designed (Figure 6). As explained above in detail, a well-defined degree of corrosion predamage by chloride-induced pitting is applied to the wires to create the acidic pit solution. Then, the potential is set to a level not far above what we may expect in practice, driving the anodic dissolution for 24 h more. As is indicated by the data on current in Figure 6 and the derived quantities in Table 3, samples A1, A2, and A3 dissolved rather steadily and HWC was indeed replicated nicely as we see from the radiographs in Figure 7. It was even possible to discriminate the weak differences in susceptibility by $A1 > A3 > A2$. By contrast, wires from C passivated readily under the

selected conditions and their damage remained limited to pitting corrosion and just very short sections of HWC, mostly caused by the predamage.

The good repassivation behavior of C material compared to A variants may be surprising, since, according to the data on magnetizability (Table 2), C wires contain much more martensite than A-type material. This points to the importance of martensite distribution and crystal orientation for susceptibility to HWC and the probability for repassivation, respectively. EBSD investigation indeed reveals significant differences in microstructure and texture between the investigated A1 and C wires: The A1 sample shows a typical fcc wire drawing microstructure and texture with $\langle 111 \rangle$ and $\langle 100 \rangle$ components while the C sample shows a twisted microstructure with a much weaker texture that significantly deviates from the more ideal wire drawing texture components in the A1 sample. Sample C exhibits a significantly higher martensite fraction than sample A1, both in the core and rim regions. Sample A1 shows a fine distribution of continuous martensite domains elongated in the drawing direction, whereas sample C exhibits a patchy distribution of martensite.

The elongated continuous domains of the more reactive martensite in A1 wires may have contributed to the preferential axial growth direction of corrosion, compared to the more patchy distribution in C material. However, this is also accompanied by a rather aligned crystal orientation of the austenite in A1, which must be considered an additional factor for the directed spreading of metal dissolution since the corrosion rate of austenite is known to depend on the attacked crystal face.^[19] In the twisted microstructure of C, however, the likelihood of the corrosion front meeting a less reactive crystal face is higher and consequently, it is also for repassivation. As a result, the texture in the wires of A1 compared to that of C seems to promote the axially directed corrosion of HWC, and not the amount but rather the elongated continuous shape of the martensite domains is relevant. An additional factor influencing the growth pattern of corrosion may be seen in residual stresses.^[18,19] Their level, direction, and distribution must also be expected to depend on the production technology of wires, and finally ropes.

4 | CONCLUSIONS

Wires of ropes made from nominally austenitic SS alloys such as AISI 316/1.4401 must contain significant amounts of α' -martensite to meet the requirements on mechanical strength. This martensite is introduced by cold working during wire drawing.

The martensite content was found not to increase the susceptibility to initiation of chloride-induced pitting corrosion at the passive surface, but it may have a strong influence on the ability of the material to repassivate from active corrosion. The readiness for repassivation is considered important in a SS rope, where fretting between the wires during dynamic loading is expected to initiate corrosion processes which are supported by the inherent crevice configuration.

No correlation between the amount of martensite and the steel's ability to repassivate was observed. Rather the distribution, size, shape, and crystal orientation of austenite and the related α' -martensite, that is, the texture of the material, appear decisive for the repassivation behavior and the growth direction of active corrosion, respectively. The samples from two different producers investigated here exemplify the existence of very different microstructures and crystallographic textures in commercial rope products, indicating different production technologies.

A crystallographic texture characteristic for uni-directional wire drawing was found to promote active corrosion and its preferential axial spreading. This appears supported by continuous martensite domains, finally resulting in HWC. By contrast, a patchy appearance of martensite in the austenitic matrix, and broad distribution of crystal orientations seem to enhance significantly the ability to repassivate by arresting the corrosion progress with barriers of gradually more resistant crystals or crystal faces, limiting corrosion to pits. Further possible influence from the level, direction, and distribution of residual stresses left from wire and rope production should not be neglected.

Since HWC in ropes may cause loss of load-carrying wires over quite some length (up to ca. 20 cm was observed in the field), a corresponding loss of strength must be considered. On the other hand, pitting, if not too dense, creates just local damage to wires and the load-carrying capability of the rope is not so much impaired due to the load distribution via friction between the remaining wire bodies. Thus, ropes made from SS wires susceptible to HWC are expected to bear a higher risk for structural failure, particularly in seawater applications. The electrochemical test for HWC as was introduced here may be the basis for assessing the susceptibility to HWC of SS wires.

ACKNOWLEDGMENTS

This research did not receive funding. For their interest and kind support, the authors are grateful to Johannes Zbiral (TU Wien) for contributing XRF analyses, Günther Ball and Matea Ban (TU Wien) for carrying out electrochemical tests, Susanne Strobel and Edith Asiemo

(TU Wien) for metallographic preparation, Werner Artner (TU Wien X-Ray Center) and Grupo de Altas Presiones y Espectroscopía (Universidad de Cantabria) for doing XRD, the Vienna micro-CT Lab (University of Vienna) for taking the X-ray photos. One of us (R. Schuster) gratefully acknowledges financial support from the Austrian Federal Ministry for Digital and Economic Affairs and the National Foundation for Research, Technology, and Development. The authors acknowledge TU Wien Bibliothek for financial support through its Open Access Funding Program.

CONFLICT OF INTEREST STATEMENT

The authors declare no conflict of interest.

DATA AVAILABILITY STATEMENT

Research data are not shared.

ORCID

Paul Linhardt  <http://orcid.org/0000-0002-4523-2185>

Maria V. Biezma  <https://orcid.org/0000-0002-0709-7656>

Roland Haubner  <https://orcid.org/0000-0002-6489-1338>

Roman Schuster  <https://orcid.org/0000-0002-3650-5217>

Tomasz Wojcik  <https://orcid.org/0000-0001-5091-5215>

REFERENCES

- [1] T. J. Lennox Jr., *NRL Memorandum Report 2045*, Naval Research Laboratory, Washington DC, USA **1969**.
- [2] DIN 81249-2, *Corrosion of Metals in Sea Water and Sea Atmosphere – Part 2: Free Corrosion in Sea Water; Text in German and English*, Deutsches Institut für Normung e. V., Beuth Verlag GmbH, Berlin, Germany **2013**.
- [3] DIN EN 10264-4, *Steel Wire and Wire Products – Steel Wire for Ropes – Stainless Steel Wire, German Version*, Deutsches Institut für Normung e. V., Beuth Verlag GmbH, Berlin, Germany **2012**.
- [4] DIN EN 10088-3, *Stainless Steels - Technical Delivery Conditions for Semi-Finished Products, Bars, Rods, Wire, Sections and Bright Products of Corrosion Resisting Steels for General Purposes, German Version*, Deutsches Institut für Normung e. V., Beuth Verlag GmbH, Berlin, Germany **2014**.
- [5] G. F. Vander Voort, *Metallography—Principles and Practice*, 3rd ed., ASM International, Materials Park, USA **2004**.
- [6] DIN EN ISO 1273, *Corrosion of Metals and Alloys – Electrochemical Potentiokinetic Reactivation Measurement Using the Double Loop Method (based on Čihal's Method)*, German Version, Deutsches Institut für Normung e. V., Beuth Verlag GmbH, Berlin, Germany **2008**.
- [7] H. Shaikh, N. Sivaibharasi, B. Sasi, T. Anita, R. Amirthalingam, B. P. C. Rao, T. Jayakumar, H. S. Khatak, B. Raj, *Corros. Sci.* **2006**, *48*, 1462.
- [8] DIN 50905-4, *Corrosion of Metals – Corrosion Testing – Performance of Chemical Corrosion Experiments Without*

Mechanical Stresses in Liquids in the Laboratory, Deutsches Institut für Normung e. V., Beuth Verlag GmbH, Berlin, Germany **2018**.

- [9] V. A. Nguyen, R. C. Newman, N. J. Laycock, *J. Electrochem. Soc.* **2022**, *169*, 081503.
- [10] B. J. Little, J. S. Lee, R. I. Ray, *Electrochim. Acta* **2008**, *54*, 2.
- [11] P. Linhardt, S. Kühner, G. Ball, M. V. Biezma, *Mater. Corros.* **2018**, *69*, 358.
- [12] A. T. English, G. Y. Chin, *Acta Metall.* **1965**, *13*, 1013.
- [13] A. D. Rollett, S. I. Wright, *Texture and Anisotropy: Preferred Orientations in Polycrystals and their Effect on Materials Properties*, Cambridge University Press, Cambridge, UK **1998**, pp. 178.
- [14] G. Kurdjumow, G. Sachs, *Z. Phys.* **1930**, *64*, 325.
- [15] Z. Nishiyama, *Sci. Rep. Tohoku Univ.* **1934**, *23*, 637.
- [16] D. A. Porter, K. E. Easterling, M. Y. Sherif, *Phase Transformations in Metals and Alloys*, 4th ed., CRC Press, Boca Raton **2021**.
- [17] H. J. Keller, G. Herbsleb, F. Kleinfeld, B. Pfeiffer, *Werkst. Korros.* **1981**, *32*, 157.
- [18] B. Ravi Kumar, R. Singh, B. Mahato, P. K. De, N. R. Bandyopadhyay, D. K. Bhattacharya, *Mater. Charact.* **2005**, *54*, 141.
- [19] P. T. Brewick, N. Kota, A. C. Lewis, V. G. DeGiorgi, A. B. Geltmacher, S. M. Qidwai, *Corros. Sci.* **2017**, *129*, 54.

How to cite this article: P. Linhardt, M. V. Biezma, R. Haubner, R. Schuster, T. Wojcik, *Mater. Corros.* **2023**;74:818–830.
<https://doi.org/10.1002/maco.202213699>